Eemian interglacial reconstructed from a Greenland folded ice core

NEEM community members*

*A full list of authors appears at the end of this paper.

Abstract

A new Greenland ice core, the NEEM core, reaches back to the last interglacial, the Eemian, 130-115 ka (thousand years before year 1950), a period warmer than our current interglacial, and documents the Greenland climate and ice sheet response to Arctic warming. Here, the stratigraphy of the deep NEEM ice, spanning the major part of the Eemian, is reconstructed from folded ice using globally-homogenous parameters known from dated Greenland and Antarctic ice core records. The warmest Greenland surface temperatures found at NEEM are 8±4^{o}C warmer than the mean of the last millennium) are estimated from water stable isotopes at the onset of the Eemian (126 ka), followed by a gradual cooling trend very likely driven by summer insolation. During the Eemian the thickness of the NW Greenland ice sheet decreased by 400±250 m reaching surface elevations of 130±300 m lower than the present at 122 ka. The findings show a modest response of the Greenland ice sheet to the significant warming in the early Eemian. In addition, the ice core data at NEEM reveal significant surface melt during the Eemian. During the exceptional heat over Greenland in July 2012 melt layers formed at NEEM. With additional warming surface melt might become more common in the future.

Introduction

A 2540 m long ice core was drilled from 2008-2012 through the Greenland ice at NEEM (77.45°N, 51.06°W, surface elevation 2450m, mean annual temperature -29^{o}C, accumulation 0.22 m ice equivalent./yr). The top 1419 m from the current interglacial, the Holocene, and the glacial ice below can be matched to the NGRIP GICC05 extended time scale [1,2] down to 2206.7 m (108 ka). Below this, the ice is disturbed and folded but it contains zones with relatively high water stable isotope ($\delta^{18}O_{ice}$, a proxy for condensation temperature) values indicating that it stems from the last interglacial, the Eemian 130-115 ka (Figure 1). Near bedrock, low $\delta^{18}O_{ice}$ values suggest ice layers from glacial periods most likely from the glacial period prior to the Eemian. The lowest 5 m of the ice core contain accreted ice, with 1 to 20 cm thick dark layers containing high concentrations of basal material. In this study information from the Eemian period of the NEEM ice core will be used to constrain the surface elevation and temperature of this warm climate period. Measurements of stable water isotopes in the ice ($\delta^{18}O_{ice}$) and CH_4, N_2O concentrations, isotopes $\delta^{15}N$ of N_2 and $\delta^{18}O$ of O_2 ($\delta^{18}O_{atm}$) and the air content have been measured from the air bubbles trapped in the ice (details in the Suppl. Mat.). In addition ice rheology of the ice, radio echo sounding (RES) images and surface and ice temperatures are used in the interpretation.

Reconstruction of the climate records

Stratigraphic disruptions are identified from discontinuities of $\delta^{18}O_{ice}$ at depths of 2209.60 m, 2262.15 m, 2364.45 m and 2432.19 m. Corresponding shifts in gas concentrations are found at these depths, so no significant depth offset is observed as expected from the bubble enclosure process. (Figure1). Possible discontinuities below 2432.19 m have not been investigated. This points to stratigraphic disturbances at these depths. The records of CH_4 concentrations and $\delta^{18}O_{atm}$ are also disturbed and are not identical to the globally-homogenous signals documented at the nearby NGRIP ice core which contains 123 ka of undisturbed stratigraphy and the EDML Antarctic ice core, which reaches back more than 135 ka [3-6]. Measurements of N_2O, $\delta^{15}N$ and air content in the NEEM ice below 2200 m further confirm these discontinuities.

NEEM data reveal spikes in CH_4 and N_2O records between depths of 2370 m and 2418 m which are too rapid to be explained by climatic variability and coincide with lower air content in the ice. These characteristics point to surface melting or wet surface conditions. Indeed, surface melting or percolating rain reduces the firn air content and allows in situ production of CH_4 and N_2O. This hypothesis is supported by results in the near-surface ice from the warmer south Greenland Dye3 ice core (Figure S9 in Supp. Mat. mean annual temperature -21^{o}C) and by measurements of noble gases over the NEEM spikes, that also support the hypothesis of melting surface layers (Figure S8 in Supp. Mat.). The lack of parallel variability in $\delta^{18}O_{ice}$, $\delta^{15}N$ or $\delta^{18}O_{atm}$ suggests that these parameters are uninfluenced by surface melting. The spikes occur in the warmest interval at the depositional location indicated by water isotopes ($\delta^{18}O_{ice}$>-33 ‰). The current water isotope mean value of the recent millennium is -33.6‰ at NEEM and very few melt layers are found in the ice core prior to year 1995[7]. During our NEEM field campaigns (2007-2012), the NEEM mean July surface air temperature has been up to -5.4^{o}C (with annual mean values $\delta^{18}O_{firn}$ > -33‰[8]) and ice cores and snow pits studies show that episodic melt events occur. During July 12th -15th 2012, the exceptional heat wave encountered over Greenland produced large surface melt over 97% of the Greenland ice sheet, leaving a strong fingerprint in NEEM in form of 5-6 cm thick melt layers 50-70 cm below the surface.

For depths of 2201.10 - 2432.19 m, the NEEM records of $\delta^{18}O_{atm}$ and the subset of CH_4 values not corrupted by surface melting are matched with globally-homogenous signals of these values observed from other ice cores [6,9,10]. For younger ice, the nearby NGRIP $\delta^{18}O_{ice}$ record is used as a reference temperature target for synchronization by assuming simultaneous abrupt climate changes at the transitions between stadials and interstadials[11] (Figures S3 and S4, Supp. Mat.).

In Figure 2, the reconstructed NEEM records are shown on the EDML1 time scale[12] and compared to the NGRIP (light grey) and EDML (dark grey) records. The zones 1 to 5, identified on Figure 1 map onto the time scale as coherent pieces. Zone 1 is folded such that the records are mirrored and repeated, zone 2 and zone 3 cover identical time periods, both inverted, while zone 4 (with melt-related spikes) and zone 5 are undisturbed and contain the major part of the ice from the Eemian (128.5-115 ka) (Figures 2 and 3ab). It cannot be ruled out that small disruptions or folds are present within the individual zones. The reconstructed records, however, show no unexpected discontinuities in the zones 1-5 in all other measured parameters such as $\delta^{15}N$ (Figure 2), dust or electrical properties. As the time scale is transferred from the EDML ice core by matching it to the globally-homogenous signals, small undetectable disruptions will not influence the conclusions based on the parameters presented here. The reconstruction is unambiguous and no other solution exists to match the NEEM $\delta^{18}O_{atm}$ and the uncorrupted CH_4 values simultaneously to EDML and NGRIP undisturbed records. No ice from 108 to 114 ka can be found in the NEEM ice core, while the ice layer from 115 to 118 ka is found three times (zones 2, 3 and 4), two of which are inverted.

The northern hemisphere temperatures are known to vary in parallel with the atmospheric CH_4 concentration[13,14] which is seen to increase abruptly into the warm Eemian period at 128 ka at EDML. This is evidence that no substantial warm phases of the NEEM Eemian record are missing before 128.5 ka. Ice from below 2450 m (zone 6) appears to be too disturbed to reconstruct an age scale based on the data available at present. The very low (glacial) $\delta^{18}O_{ice}$ values (-44.9 ‰ at 2476 m) are first found again in the record above 2011 m. The ice layering at the NEEM site is undisturbed above 2200 m (Figure 3g), so the section below 2476 m is believed to contain ice older than 128.5 ka from Marine Isotopic Stage (MIS) 6 and we may speculate that the increased levels of $\delta^{18}O_{ice}$, CH_4 and N_2O at 2480 m might be from MIS-7 interglacial.

The disturbed and folded ice

Radio echo sounding (RES) data were collected in North Greenland 2011 and 2012 with a Multichannel Coherent Ice-penetrating Radar Depth Sounder/Imager[15,16]. The radar data show continuous and undisturbed internal layers (isochrones) to a depth of about 2200 m in the NEEM region, in agreement with the ice core observations[17]. Below 2200 m, internal layers become fuzzy and less continuous: undulations and even overturned folds and shearing of basal material are observed (Figure 3fg and Suppl. Mat.). The transition between clear and fuzzy layers often appears at the interface between ice from the glacial and Eemian periods. Very large differences in ice rheological properties are documented between glacial ice with crystal sizes of 1.5 mm and a strong preferred vertical c-axis orientation and Eemian ice with crystal sizes of 25 mm and multiple maxima fabrics (Figure 3cd). The viscosities of these two types of ice differ by a factor of 50-100[18-21], allowing glacial ice to deform very easily, while the interglacial ice is more rigid. The missing, folded, and inverted parts of the ice are from the interface between the relatively rigid Eemian and the early glacial 114-108 ka immediately above it, supporting the idea that the glacial ice over the harder Eemian ice deforms. The broken record at 128.5 ka can be explained by contrasting the deformation properties of the underlying ice from the previous glacial period and the Eemian ice. It should be noted that the discontinuous and folded structures of the GRIP and GISP2 ice cores also occur for ice older than 105 ka[9,10]. The consistency of the radar images and deep ice core results at NEEM is a breakthrough result and it demonstrates that radar imaging can now be used to predict folded ice layering. This opens the potential for a systematic reconstruction of the Eemian Greenland ice sheet layering from new radar imaging. Assimilation of such data in ice sheet models may lead to much improved histories of the configuration of the ice sheet in the past improving our ability to predict the future evolution of the ice sheet.

Climate reconstruction from the observed records

The reconstructed Eemian sequence (128.5-114 ka, Figure 2)) allows for initial climate interpretations of this period. As mentioned above, the regular occurrence of melt features at 127-

118.3 ka indicates of warmer temperatures at the depositional surface locations of the ice than the mean of the recent millennium at NEEM. This is independently confirmed by the decrease of $\delta^{15}N$ in this zone, which is indicative of ~5^{o}C warmer mean annual firn temperatures at the depositional site [22,23](Supp. Mat. in figure S7). Between 128.5 ka and 126.0 ka, $\delta^{18}O_{ice}$ increases from -35 ‰ to -31.4 ‰ while EDML $\delta^{18}O_{ice}$ values slowly drop from those of the early Antarctic warm period[24]. This bipolar see-saw behavior suggests that inter hemispheric heat redistribution by the Atlantic Meridional Overturning Circulation[25] is taking place within the Eemian interglacial period as also observed during the last northern hemisphere deglaciation 19-11 ka [24-27]. Before surface melt began between 128.5-126.7 ka, the air content at the depositional site had a stable level of 85 ml/kg compared to the present level of 97.5 ml/kg. When corrected for changing local summer insolation[28-30], the air content difference suggests a surface elevation at the depositional site, 540±300 m higher at the onset of the Eemian (128 ka) than the surface elevation at NEEM today[28,31-33]. The locations of the depositional sites of the Eemian ice found in the NEEM ice core, are modeled using a nested 3 dimensional flow model[34] (Supp. Mat., Figure 1a,). A second model used to date the NEEM ice core reaches similar locations[35] within 20 km. At present the surface elevation at the depositional site of the 128 ka old ice (205±20 km upstream from NEEM) is 330±50 m higher than the present at NEEM[33,34]. The surface elevation increase of 210±350 m at the 128 ka depositional site (Figure 4c, blue) is the difference between the elevation at 128 ka (540±300m) and the present elevation (330±50m), both related to the present elevation at NEEM. This surface elevation increase is expected at the onset of a warm climatic period due to generally increased precipitation and mass balance before the central part of the ice sheet adjusts to the warmer climate by increased ice flow. This is also established at the onset of the present interglacial at 11.7 ka[32].

In the period 127-118.3 ka where surface melt occurred, the air content in the ice was highly variable and cannot directly be used for ice elevation reconstructions (Figure 2, shaded zone). We

can tentatively predict elevation changes through the Eemian climate period by connecting the two air content levels before and after the melt zone (Figure 4b), after correction for summer insolation which accounts for 50 % of the observed change (Figure 4c, Supp. Mat.). At 126 ka the surface elevation was 45±350 m higher than the present. The $\delta^{18}O_{ice}$ increased to -31.4 ‰ at 126 ka exceeding the current mean value of the recent millennium of -33.6 ‰ (at the NEEM site) and the current mean value of 35.0 ‰ at the depositional site[32,33] (Suppl. Mat, section 2). Using the temperature/isotope relation of 2.1±0.5 K/ ‰ (Calibrated using data from the present interglacial[32]), the 3.6 ‰ 126 ka anomaly implies that precipitation weighted surface temperatures was 7.5±1.8 ^{o}C warmer at the depositional site compared to the last millennium. Note that modeled location of the depositional site is only required to compare the 126 ka data to the present day data at the depositional site. When further correcting for the more uncertain elevation change of 45±350 m at the 126 ka depositional site using a lapse rate of 7.5±0.5 K/km, the fixed-elevation temperature increase here is 8±4 ^{o}C (Figure 4a, red). Our data depict a gradual cooling until 110 ka (Figure 4a, red curve).

The reconstructed precipitation-weighted annual temperature changes are remarkably high. In general, warmer summer temperatures are reported from palaeorecords[36,37], and a few find as high temperatures at 126 ka on high Arctic latitudes as those reported from NEEM[38-40]. Climate models equipped with water stable isotopes point to a limited (1°C) seasonality bias caused by a stronger enhancement of temperature and precipitation in summer than in winter[41-43]. A large spread in temperature has been reported among simulations of the Last Interglacial Climate, which appear to systematically underestimate North Atlantic/Arctic warming, possibly due to missing vegetation and ice sheet feedbacks[37,42,43].

Within 6000 years, from 128 ka to 122 ka, the surface elevation is estimated to decrease from 210±350 m above to 130±300 m below the present surface elevation, which translates into a moderate ice thickness change of 400±350 m after accounting for isostatic rebound. Based on this

estimate, the ice thickness at NEEM decreased by an average of 7±4 cm per year between 128 and 122 ka and stayed at this level until 117-114 ka, long after surface melt stopped and when temperatures fell below modern levels.

Even with elevation changes of only about 10% of the ice thickness at the center of the ice sheet as reported here, substantial melting can cause significant reduction of ice thickness near margins that in turn reduces the volume of the Greenland ice sheet. While the documentation of ice thickness at one location of the Greenland ice sheet cannot constrain the overall ice sheet changes during the last interglacial period, the NEEM data can only be reconciled with Greenland ice sheet simulations[30] that point to a modest contribution (2 m) to the observed 4-8 m Eemian sea level high stand[44,45]. For comparison, no ongoing elevation change has so far been detected in the area with elevations above 2000m in North Greenland during the last decades[46]. These findings strongly imply that Antarctica must have contributed significantly to the Eemian sea level rise[47].

Despite the complex ice flow, the disturbed record of the deep ice in the NEEM ice core can be unambiguously reconstructed. The anatomy of the last interglacial showed that Greenland temperature peaked at the onset of the Eemian, 126 ka, with temperatures (at fixed elevation) 8±4 ^{o}C warmer than the average of the recent millennium and multiple indications of summer melt. Temperature gradually decreased during the interglacial, very likely due to the strong local summer insolation trend. The surface elevation first increased due to increased mass balance to 210±350 m above the present at 128 ka, then decreased to 130±300 m below the present elevation around 122 ka BP. Our results provide multiple new targets to constrain coupled climate/ice sheet models. Our record together with recent observations of rain fall and strong surface melting in July 2012 at NEEM show that conditions are conductive to the start of melt layers formation at NEEM, with the 2010-2012 mean annual surface temperatures being 1-2 ^{o}C above the 1950-1980 average.

Our results have implications first for ice deformation near bedrock, and second for the Greenland ice sheet response to climate change. The combination of high-resolution radar echo data and NEEM glacial-interglacial ice layers brings new knowledge on the near-bed deformation of ice. We believe that the folding and disturbance we observe near the bed is strongly related to the hard deformation properties of the interglacial ice. This offers an alternative explanation for the large anomalies in radar profiles recently observed both under the Antarctic and the Greenland ice sheet, which were previously attributed to refrozen basal water[48].

Methods Summary

Measurements of stable water isotopes in the ice ($\delta^{18}O_{ice}$), CH_4, N_2O concentrations and the isotopes $\delta^{15}N$ of N_2 and $\delta^{18}O_{atm}$ of O_2, noble gases and the air content have been measured from the extracted air from the air bubbles in the ice, all using well-described methods are presented in section 1 of the Supp. Mat. Models calculating temperatures from water isotopes, elevation changes from air content and temperature changes from $\delta^{15}N$ values have been calibrated using observations from the Present Interglacial. The early phase of the Present Interglacial is documented at high resolution, and used to characterize processes in a context of enhanced Greenland temperatures compared to present day, although not as warm as during the Last Interglacial.

1 *Wolff EW, C. J., Blunier T, Rasmussen SO, Svensson A. Millennial-scale variability during the last glacial: The ice core record. Quaternary Science Reviews* ***29****, 2828-2838, doi:10.1016/j.quascirev.2009.10.013 (2010).*

2 *Svensson, A. et al. A 60 000 year Greenland stratigraphic ice core chronology. Climate of the Past* ***4****, 47-57 (2008).*

3 *Andersen, K. K. et al. High-resolution record of Northern Hemisphere climate extending into the last interglacial period. Nature* ***431****, 147-151 (2004).*

4 *Barbante, C. et al. One-to-one coupling of glacial climate variability in Greenland and Antarctica. Nature **444**, 195-198, doi:10.1038/nature05301 (2006).*

5 *Schilt A, B. M., Blunier T, Schwander J, Spahni R, Fischer H, Stocker TF. Glacial–interglacial and millennial-scale variations in the atmospheric nitrous oxide concentration during the last 800,000 years. Quaternary Science Reviews **29**, 182-192, doi:10.1016/j.quasirev.2009.03.011 (2010).*

6 *Capron E, L. A., Lemieux-Dudon, Schilt A, Masson-Delmotte V, Buiron D, Chappellaz J, Dahl-Jensen D, Johnsen S, Leuenberger M, Loulergue L, Oerter H. Synchronising EDML and NorthGRIP ice cores using δ18O of atmospheric oxygen (δ18Oatm) and CH4 measurements over MIS5 (80–123 kyr). Quaternary Science Reviews **29**, 222-234, doi:10.1019/j.quasscirev.2009.07.014 (2010).*

7 *Steen-Larsen HC, M.-D. V., Sjolte J, Johnsen SJ, Vinther MB, Bréon FM, Clausen HB, Dahl-Jensen D, Falourd S, Fettweis X, Gallee H, Jouzel J, Kageyama M, Lerche H, Minster B, Picard G, Punge HJ, Risi C, Salas D, Schwander J, Steffen K, Sveinbjornsdottir AE, Svensson A, White J. Understanding the climatic signal in the water stable isotope records from the NEEM shallow firn/ice cores in northwest Greenland. Journal of Geophysical Research Atmospheres **116**, 20, doi:10.1029/2010JD014311 (2011).*

8 *Buchardt, S. L., Clausen, H. B., Vinther, B. M. & Dahl-Jensen, D. Investigating the past and recent O18-accumulation relationship seen in Greenland ice cores. Climate of the Past (submitted).*

9 *Landais, A. et al. A tentative reconstruction of the last interglacial and glacial inception in Greenland based on new gas measurements in the Greenland Ice Core Project (GRIP) ice core. Journal of Geophysical Research-Atmospheres **108**, doi:10.1029/2002jd003147 (2003).*

10 *Suwa, M., J. C. von Fischer, Bender, M. L., Landais, A. & Brook, E. J. Chronology reconstruction for the disturbed bottom section of the GISP2 and the GRIP ice cores:*

Implications for Termination II in Greenland. Journal of Geophysical Research ***111****, D02101, doi:02110.01029/02005JD006032 (2006).*

11 Johnsen, S. J. et al. Oxygen isotope and palaeotemperature records from six Greenland ice-core stations: Camp Century, Dye-3, GRIP, GISP2, Renland and NorthGRIP. Journal of Quaternary Science ***16****, 299-307 (2001).*

12 Ruth, U. et al. "EDML1": a chronology for the EPICA deep ice core from Dronning Maud Land, Antarctica, over the last 150 000 years. Climate of the Past ***3****, 475-484 (2007).*

13 Caillon, N., Jouzel, J., Severinghaus, J. P., Chappellaz, J. & Blunier, T. A novel method to study the phase relationship between Antarctic and Greenland climate. Geophysical Research Letters ***30****, doi:10.1029/2003GL017838 (2003).*

14 Chappellaz, J. et al. Synchronous changes in atmospheric CH_4 and Greenland climate between 40 and 8 kyr BP. Nature ***366****, 443-445 (1993).*

15 Rodriguez-Morales, F. et al. Advanced Multi-Frequency Radar Instrumentation for Polar Research. IEEE Transactions on geoscience and Remote Sensing ***submitted*** *(submitted).*

16 Leuschen, C. et al. The CReSIS Radar Suite for Measurements of the Ice Sheets and Sea Ice during Operation Ice Bridge. American Geophysical Union Fall Meeting, December 13-17 (2010).

17 Buchardt, S. & Dahl-Jensen, D. At what depth is the Eemian layer expected to be found at NEEM? Annals of Glaciology ***48****, 100-102, doi:10.3189/172756408784700617 (2008).*

18 Dahl-Jensen, D. & Gundestrup, N. in The Physical Basis of Ice Sheet Modelling. (Proceedings of the Vancouver Symposium, August 1987) IAHS Publ. No. 170 (ed E. Waddington) 31-43 (1987).

19 Dahl-Jensen, D. & Gundestrup, N. S. Derivation of flow-law properties from bore-hole tilt data: Discussion of the Dye 3, Camp Century, and Byrd Station bore-hole results (Abst). Annals of Glaciology ***12****, 200-201 (1989).*

20 *Azuma, N. & Higashi, A. Mechanical properties of Dye 3 Greenland deep ice cores. Annals of Glaciology **5**, 1-8 (1984).*

21 *Jacka, T. H. Laboratory studies on relationships between ice crystal size and flow rate. Cold Regions Science and Technology **10**, 31-42 (1984).*

22 *Goujon, C., Barnola, J.-M. & Ritz, C. Modeling the densification of polar firn including heat diffusion: Application to close-off characteristics and gas isotopic fractionation for Antarctica and Greenland sites. Journal of Geophysical Research **108**, 4792, doi:4710.1029/2002JD003319 (2003).*

23 *Severinghaus, J. P., Grachev, A. & Battle, M. Thermal fractionation of air in polar firn by seasonal temperature gradients. Geochemistry, Geophysics, Geosystems **2**, doi: 10.1029/2000GC000146 (2001).*

24 *Masson-Delmotte V, S. B., Blunier T, Cattani O, Chappellaz J, Cheng H, Dreyfus G, Edwards RL, Falourd S, Govin A, Kawamura K, Johnsen SJ, Jouzel J, Landais A, Lemieux-Dudon B, Lourantou A, Marshall G, Minster B, Mudelsee M, Pol K, Röthlisberger R, Selmo E, Waelbroeck C. Abrupt change of Antarctic moisture origin at the end of Termination II. PNAS **107**, 12091-12094, doi:10.1073/pnas.0914536107 (2010).*

25 *Stocker, T. F. & Johnsen, S. J. A minimum thermodynamic model for the bipolar seesaw. Paleoceanography **18**, 1087, doi:1010.1029/2003PA000920 (2003).*

26 *Pedro, J. B. et al. The last deglaciation: timing the bipolar seesaw. Climate of the Past **7**, 671-683, doi:10.5194/cp-7-671-2011 (2011).*

27 *Stenni, B. et al. Expression of the bipolar see-saw in Antarctic climate records during the last deglaciation. Nature Geoscience **4**, 46-49 (2011).*

28 *Raynaud, D. et al. The loca linsolation signature of aircontent in Antarcticice. A new step toward an absolute dating of ice records. Earth and Planetary Science Letters **261**, 337-349, doi:10.1016/j.epsl.2007.06.025 (2007).*

29 *Berger, A., Loutre, M. F. & Laskar, J. Stability of the Astronomical Frequencies Over the Earth's History for Paleoclimate Studies. Science **255**, 560-566, doi:10.1126/science.255.5044.560 (1992).*

30 *van de Berg, W. J., van den Broeke, M., Ettema, J., van Meijgaard, E. & Kaspar, F. Significant contribution of insolation to Eemian melting of the Greenland ice sheet. Nature Geoscience **4**, 679-683, doi:10.1038/ngeo1245 (2011).*

31 *Raynaud, D., Chappellaz, J., Ritz, C. & Martinerie, P. Air content along the Greenland Ice Core Project core: A record of surface climatic parameters and elevation in central Greenland. Journal of Geophysical Research **102**, 26607-26613 (1997).*

32 *Vinther, B. M. et al. Holocene thinning of the Greenland ice sheet. Nature **461**, 385-388 (2009).*

33 *Bamber, J. L., Layberry, R. L. & Gogineni, S. A new ice thickness and bed data set for the Greenland ice sheet 1. Measurement, data reduction, and errors. Journal of Geophysical Research-Atmospheres **106**, 33773-33780 (2001).*

34 *Huybrechts, P., Rybak, O., Pattyn, F., Ruth, U. & Steinhage, D. Ice Thinning, upstream advection, and non-limatic biases for the upper 89% of the EDML ice core from a nested model of the Antarctic ice sheet. Climate of the Past **3**, 577-589 (2007).*

35 *Buchardt, S. L. Basal melting and Eemian ice along the main ice ridge in northern Greenland, Dissertation, University of Copenhagen (http://www.iceandclimate.nbi.ku.dk/publications/theses/). (2009).*

36 *Otto-Bliesner, B. L. et al. Simulating arctic climate warmth and icefield retreat in the last interglaciation. Science **311**, 1751-1753, doi:10.1126/science.1120808 (2006).*

37 *Lunt, D. J. et al. A multi-model assessment of last interglacial temperatures. Climate of the Past Discussions **8**, 3657-3691, doi:0.5194/cpd-8-3657-2012 (2012).*

38 *Axford, Y. et al. Chironomids record terrestrial temperature changes throughout Arctic interglacials of the past 200,000 yr. Geological Society of America Bulletin **123**, 1275-1287, doi:10.1130/B30329.1 (2011).*

39 *Francis, D. R., Wolfe, A. P., Walker, I. R. & Miller, G. F. Interglacial and Holocene temperature reconstructions based on midge remains in sediments of two lakes from Baffin Island, Nunavut, Arctic Canada. Palaeogeography, palaeoclimatology, palaeoecology **236**, 107-124 (2006).*

40 *Turney, C. S. M. J., R. T. Does the Agulhas Current amplify global temperatures during super-interglacials? Journal of Quaternary Science **25**, 839-843, doi:DOI: 10.1002/jqs.1423 (2010).*

41 *Born, A. N., K.H. Melting of Northern Greenland during the last interglacial. The Cryosphere Discuss. **5**, 3517-3539, doi:10.5194/tcd-5-3517-2011 (2011).*

42 *Masson-Delmotte, V. et al. Sensitivity of interglacial Greenland temperature and δ18O: ice core data, orbital and increased CO2 climate simulations. Climate of the Past **7**, 1041-1059, doi:10.5194/cp-7-1041-2011 (2011).*

43 *Masson-Delmotte, V. et al. EPICA Dome C record of glacial and interglacial intensities. Quaternary Science Reviews **21**, 113–128 (2010).*

44 *Kopp, R. E., Simons, F. J., Mitrovica, J. X., Maloof, A. C. & Oppenheimer, M. Probabilistic assessment of sea level during the last interglacial stage. Nature **462**, 863-U851, doi:10.1038/nature08686 (2009).*

45 *Dutton, A. & Lambeck, K. Ice Volume and Sea Level During the Last Interglacial Science **337**, 216-219, doi:10.1126/science.1205749 (2012).*

46 *Dahl-Jensen, D. et al. in Snow, Water, Ice and Permafrost in the Arctic (SWIPA): Climate Change and the Cryosphere (ed AMAP) 8-1 - 8-68 (AMAP, 2011).*

47 *Bradley, S. L., Siddall, M., Milne, G. A., Masson-Delmotte, V. & Wolff, E. Where might we find evidence of a Last Interglacial West Antarctic Ice Sheet collapse in Antarctic ice core records? Global and Planetary Change* ***88-89****, 64-75 (2012).*

48 *Bell, R. E. et al. Widespread Persistent Thickening of the East Antarctic Ice Sheet by Freezing from the Base. Science* ***331****, 1592-1595, doi:10.1126/science.1200109 (2011).*

49 *Raynaud, D. & Lebel, B. Total gas content and surface elevation of polar ice sheets. Nature* ***281****, 289-291 (1979).*

50 *Martinerie, P. et al. Air content paleo record in the Vostok ice core (Antarctica): A mixed record of climatic and glaciological parameters. Journal of Geophysical Research* ***99****, 10565-10576 (1994).*

51 *Kobashi, T. S., J.P. Barnola, J.M. 4 ± 1.5 °C abrupt warming 11,270 yr ago identified from trapped air in Greenland ice. Earth and Planetary Science Letters* ***268****, 397-407, doi:10.1016/j.epsl.2008.01.032 (2008).*

Supplementary Information accompanies the paper on *Nature's* homepage www.nature.com

Acknowledgements. *This work could not have been achieved without the many persons involved in logistics, drill developments and drilling, ice core processing and analysis, in the field and in our laboratories. NEEM is directed and organized by the Center of Ice and Climate at the Niels Bohr Institute and US NSF, Office of Polar Programs. It is supported by funding agencies and institutions in Belgium (FNRS-CFB and FWO), Canada (NRCan/GSC), China (CAS), Denmark (FIST), France (IPEV, CNRS/INSU, CEA and ANR), Germany (AWI), Iceland (RannIs), Japan (NIPR), Korea (KOPRI), The Netherlands (NWO/ALW), Sweden (VR), Switzerland (SNF), United Kingdom (NERC) and the USA (US NSF, Office of Polar Programs) and the EU programmes Past4Future and WaterundertheIce from the EU 7th Framework programme. NASA is acknowledged for the OIB 2011 program.*

Author contributions. All authors discussed results and contributed to the manuscript by providing data and/or models.

Author information. The authors declare they have no competing financial interests.

Correspondance and requests for materials should be addressed to Dorthe Dahl-Jensen (ddj@gfy.ku.dk)

*NEEM community members contributing to this paper are: D. Dahl-Jensen[1], M.R. Albert[2], A. Aldahan[3], N. Azuma[4], D. Balslev-Clausen[1], M. Baumgartner[5], A.-M. Berggren[3], M. Bigler[5], T. Binder[6], T. Blunier[1], J.C. Bourgeois[7], E.J. Brook[8], S.L. Buchardt[1], C. Buizert[1,8], E. Capron[9,10], J. Chappellaz[11], J. Chung[12], H.B. Clausen[1], I. Cvijanovic[1], S. M. Davis[13], P. Ditlevsen[1], O. Eicher[5], H. Fischer[5], D.A. Fisher[7], L. Fleet[10], G. Gfeller[5], V. Gkinis[1,20], S. Gogineni[14], K. Goto-Azuma, [15], A. Grinsted[1], H. Gudlaugsdottir[16], M. Guillevic[1,9], S.B. Hansen[1], M. Hansson[17], M. Hirabayashi[15], S. Hong[18], S.D. Hur[12], P. Huybrechts[19], C. Hvidberg[1], Y. Iizuka[17,23], T. Jenk[1], S.J. Johnsen[1], T.R. Jones[20], J. Jouzel[9], N.B. Karlsson[1], K. Kawamura[15], K. Keegan[2], E. Kettner[1], S. Kipfstuhl[21], H.A. Kjær[1], M. Koutnik[22], T. Kuramoto[15,23], P. Köhler[21], T. Laepple[21], A. Landais[9], P. Langen[1], L.B. Larsen[1], D. Leuenberger[5], M. Leuenberger[5], C. Leuschen[14], J. Li[14], V. Lipenkov[24], P. Martinerie[11], O.J. Maselli[25], V. Masson-Delmotte[9], J.R. McConnell[25], H. Miller[21], O. Mini[5], A. Miyamoto[26], M. Montagnat-Rentier[11], R. Mulvaney[10], R. Muscheler[27], A.J. Orsi[28], J. Paden[14], C. Panton[1], F. Pattyn[29], J.-R. Petit[11], K. Pol[9,10], T. Popp[1], G. Possnert[30] F. Prié[9], M. Prokopiou[31], A. Quique[11], S.O. Rasmussen[1], D. Raynaud[11], J. Ren[32], C. Reutenauer[1], C. Ritz[11], T. Roeckeman[31], J.L. Rosen[8], M. Rubino[1,33], O. Rybak[19], D. Samyn[3,4], C.J. Sapart[31], A. Schilt[5,8], A. Schmidt[1], J. Schwander[5], S. Schüpbach[5], I. Seierstad[1], J.P. Severinghaus[28], S. Sheldon[1], S.B. Simonsen[1], J. Sjolte[1], A.M. Solgaard[1], T. Sowers[34], P. Sperlich[1], H.C. Steen-Larsen[1,9], K. Steffen[35,†] , J.P.Steffensen[1], D. Steinhage[21], T. Stocker[5], C. Stowasser[1], A. S. Sturevik[3], B. Sturges[36], A. Sveinbjörnsdottir[16], A. Svensson[1], J.-L- Tison[29], J. Uetake[15], P. Vallelonga[1], R.S.W. van de Wal[31], G. van der Wel[5], B.H.

Vaughn[20], B. Vinther[1], E. Waddington[22], A. Wegner[21], I. Weikusat[21], J.W.C. White[20], F. Wilhelms[21], M. Winstrup[1], E. Witrant[37], E. Wolff[10], C. Xiao[32,38], J. Zheng[7]

Author Affiliations

1.Centre for Ice and Climate, Niels Bohr Institute, University of Copenhagen, Juliane Maries Vej 30, 2100 Copenhagen K, Denmark;

2. Thayer School of Engineering, Dartmouth University, Hanover, N.H. 03755;

3. Department of Earth Sciences, Uppsala University, Villav. 16, 752 36 Uppsala, Sweden

4. Department of Mechanical Engineering, Nagaoka University of Technology, 1603-1 Kamitomioka-machi, Nagaoka 940-2188, Japan

5. Climate and Environmental Physics, Physics Institute & Oeschger Centre for Climate Change Research, University of Bern, Sidlerstrasse 5, 3012 Bern, Switzerland;

6. IWR University of Heidelberg, Speyerer Straße 6, D-69115 Heidelberg, Germany;

7. Natural Resources Canada, Geological Survey of Canada, 601 Booth Street, Ottawa, Canada, K1A 0E8;

8. College of Earth, Ocean, and Atmospheric Sciences, Oregon State University, 104 CEOAS Admin Bldg, Corvallis OR 97331-5503, USA;

9. Laboratoire des Sciences du Climat et de l'Environnement, CEA-CNRS-UVSQ, IPSL, Bat 701 L'Orme des Merisiers, CEA Saclay 91 191 Gif sur Yvette, France;

10. British Antarctic Survey, Madingley Road, Cambridge, CB3 0ET, UK;

11. LGGE, UJF-Grenoble 1, CNRS, 64 rue Molière, BP 96, 38402 St Martin d'Hères, France;

12. Korea Polar Research Institute, Songdo Techno Park, 7-50, Songdo-dong, Yeonsu-gu, Incheon 406-840, Korea;

13. Department of Geography, College of Science, Swansea University, Singleton Park, Swansea, SA2 8PP, Wales, UK;

14. CReSIS, University of Kansas, Nichols Hall, 2335 Irving Hill Road, Lawrence, Kansas 66045, USA;

15. National Institute of Polar Research, 10-3 Midori-cho, Tachikawa, Tokyo 190-8518, Japan;

16. Institute of Earth and Sciences, University of Iceland, Sturlugata 7, IS-107, Reykjavik, Iceland;

17. Department of Physical Geography and Quaternary Geology, Stockholm University, S-106 91 Stockholm, Sweden;

18. Department of Ocean Sciences, Inha University, 100 Inha-ro, Nam-gu, Incheon 402-751, Korea;

19. Earth System Sciences & Department of Geography, Vrije Universiteit Brussel, Pleinlaan 2, B-1050 Brussels, Belgium;

20. INSTAAR, University of Colorado, Boulder, Colorado, 80309 USA;

21. Alfred Wegener Institute for Polar and Marine Research, PO Box 12 01 61, D-27515 Bremerhaven, Germany

22. Department of Earth and Space Sciences, University of Washington, Seattle WA 98195-1310 USA;

23. Institute of Mountain Science, Shinshu University, 3-1-1, Asahi, Matsumoto City 390-8621, Japan

24. Arctic and Antarctic Research Institute, St. Petersburg 199397, Russia;

25. Desert Research Institute, Nevada System of Higher Education, Reno, NV 89512, USA;

26. Institute of Low Temperature Science, Hokkaido University, Sapporo 060-0819, Japan;

27. Department of Geology, Lund University, Sölvegatan 12, SE-22362 Lund, Sweden;

28. Scripps Institution of Oceanography, UC San Diego, La Jolla, CA 92093, USA;

29. Laboratoire de Glaciologie, Université Libre de Bruxelles; CP160/03, Avenue F.D. Roosevelt 50, B-1050 Brussels, Belgium;

30. Tandem Laboratory, Uppsala University, Lägerhyddsv. 1, 751 20, Uppsala, Sweden

31. Institute for Marine and Atmospheric research Utrecht (IMAU) Utrecht University, Princetonplein 5, 3584 CC Utrecht, The Netherlands;

32. State Key Labarotory of Cryospheric Sciences, Cold and Arid Regions Environmental and Engineering Research Institute, Chinese Academy of Sciences, Lanzhou 730000, China;

33. Centre for Australian Weather and Climate Research, CSIRO Marine and Atmospheric Research, Aspendale, 3195, Victoria, Australia

34. Earth and Environment Systems Institute, Penn State University, 2217 EES Building, University Park, PA 16802, USA;

35. CIRES, University of Colorado, 216 UCB Boulder, CO 80309-0216 USA,

36. University of East Anglia, Norwich, Norfolk, NR4 7TJ, UK;

37. UJF - Grenoble 1 / CNRS, Grenoble Image Parole Signal Automatique (GIPSA-lab), UMR 5216, B.P. 46, 38402 St Martin d'Hères, France;

38. China Instiute of Climate System, Chinese Academy of Meteorological Sciences, Beijing 100081, China

Present address:

† Swiss Federal Research Institute WSL; IAC, Swiss Federal Institute of Technology (ETH); ENAC, École Polytechnique Fédéral de Lausanne

K. Steffen

Author contributions: All authors have contributed to the discussions that lead to the results presented in the paper. M.R.A, A.-M.B., C.B., K.Ke., P.M., S.B.S. and E.W. have performed analysis and interpretation of the firn processes; A. A. , D. B.-C., M.Ba., M. Bi., T.Bl., E.B., E.C., J.Cha., J. Chu.,O.E., H.F., L.F., G.G., V.G., K. G.-A., M.H., Y.I., T.J., T.R.J., J.J., K.Ka., E.K., H.A.K., T.K., A.L., V.L., O.J.M., V.M.-D., J.R.M., O.M., R.Mus., J.-R.P., K.P., G.P., T.P., M.P., D.R., C.R., T.R., J.L.R., M.R., C.J.S., A.Schi., J.S., S.Sc., J.P.Se., T.S., P.S., T.S., C.S., B.S., A. St., A.Svei., A.Sven., J.U., P.V., G.vdW., B.H.V., B.V., A.W. and F.W., have been involved in the data measurements described in detail in the Supplementary Material; N. A., T.Bi., S.K., A.M., M.M.-R., D.S., E.W. and I.W. have contributed to the understanding of the ice rheology; J.C.B. and A.Schm., investigates the biology of the ice cores; S.L.B., P.H., M.K., F.P., A.Q., C.R., O.R.,A.M.S. and R.S.W.vdW., have produced ice sheet models; H.B.C. , S.D., D.A. F., A.G., H.G., M.G., S.J.J., P.K., A.L.,T.L., D.L., M.L., S.O.R., I.S., J.P.St. and M.W. have participated in the dating of the NEEM ice core; I.C., P.D., P.L. and J.S., have produced atmosphere models; D.D.J. has performed the analysis of the data; J.W.C.W. and E.W. have communicated the discussion into the text ; S.G., N.B.K., C.L., J.L., J.P., C. P. and D.S. have participated in obtaining and interpreting the Radio Echo Sounding Images; S.B.H. and S.S. have been chef mechanic and electronic engineer on the deep ice core drill; M.G., S.H.,S.D.H., H.M., R.Mul., J.R. and C.X. have participated in the planning of the NEEM project; L.B.L. and C.H. have used a GPS net to

determine the surface velocities; E.C., A.L., A.J.O., F.P., H.-C.S.-L., K.S. and J.Z. have participated in measuring temperatures and isotopes in the firn and air; J.L.-T. has been involved in the interpretation of the basal ice.

Figure 1

Observed NEEM records. a) Map of the position of the NEEM camp including upstream depositional positions of the ice found in the NEEM ice core. The deep ice core sites NGRIP, NEEM and Camp Century and the tracks of the radio echo sounding images shown on Figure 3f and 3g (red lines) are shown on the map. b) The observed records of $\delta^{18}O_{ice}$, $\delta^{18}O_{atm}$ *(reversed scale)* CH_4, N_2O, $\delta^{15}N$ *and air content (reversed scale) from 2162 m and deeper are plotted on the NEEM depth scale below the plot. Zone 0-6 (blue: 0-2206.5 m, cyan: 2206.5-2209.6 m, green: 2209.6-2262.2 m, orange: 2262.2-2364.5 m, red: 2364.5-2418.0 m, dark red: 2418.0-2432.2 m and brown: 2432.2-2537 m) represent the sections of the NEEM ice core records with symbols marking the start (diamond)and end (square) of each zone. There is no discontinuity between zone 4 and 5 but spikes of* CH_4, N_2O *and air content occur in zone 4 (shaded grey). For comparison the NGRIP data is plotted as light grey curves on the NGRIP depth scale on top of the plot. The NEEM and NGRIP depth scale are synchronized between 2162 and 2207.6 m NEEM depths.*

Figure 2

Reconstructed records from the NEEM ice core. The reconstructed records of $\delta^{18}O_{ice}$, $\delta^{18}O_{atm}$ *(reversed scale)* CH_4, N_2O, $\delta^{15}N$ *and air content (reversed scale) on the EDML1 time scale* [12]*. Zone*

1 (cyan) is seen to contain a fold while zone 2 (green) and zone 3 (orange) are reversed and cover identical time periods. NGRIP records (light grey) and EDML records (dark grey) are included where they are available. The CH_4, N_2O and air content records contain spikes from 118.3 to 127 ka BP (shaded grey).

Figure 3

Disturbances of the deep NEEM ice. a)The reconstructed NEEM stable water isotope record (black curve) including NGRIP data between 114-108 ka BP (grey) on the EDML1 timescale that has been color coded according to age. b) The color coded dating plotted with the original data on the NEEM depth scale visualizing the discontinuities and the reversed sections. c) c-axis orientations on Schmidt diagrams for the depths 2203m, 2308 m and 2395 m and polarized light pictures of ice thin sections from the same three depths (d) demonstrate the very different ice rheology of the glacial and interglacial ice leading to different flow properties. e) Cartoon of a possible history of the formation of two overturned folds at NEEM inspired by the observed undulations in the RES images (f and g). f)-g) Center for Remote Sensing of ice Sheets (CReSIS) ice penetrating RES images from NASA Operation IceBridge campaign 2011. f) is a 52 km long line to the west that illustrates that overturning folds do occur while (MCORDIS: 20110329_02_020) g) is a 48 km long line crossing the deep drill site (MCORDIS 20110329_02_028). The NEEM site is marked on the image and two dated horizons are marked. More details can be found in the supplementary material.

Figure 4

Reconstruction of the temperature and elevation history. Reconstruction of the temperature and elevation history though the Eemian based on the stable water isotopes ($\delta^{18}O_{ice}$) and the air content records. The zone with surface melt (127-118.3 ka) is shaded in light gray. a) The measured $\delta^{18}O_{ice}$ record (black) on the constructed time scale. The average of the recent millennium -33.60‰ is marked with a thin black line. Note that the Eemian record should be compared to the last millennium at the upstream depositional site (-35.0 ‰) It is seen that the $\delta^{18}O_{ice}$ values at the depositional locations in the melt zone are above -33.0‰ (grey horizontal line). The fixed-elevation change of temperature constructed from the observed $\delta^{18}O_{ice}$, the elevation changes determined from the air content and the upstream corrections (curves below) is shown as a red curve with light red error bars using the red axis. A temperature maximum of 8±4^{o}C above the average of the recent millennium is found at 126 ka. b) : Air content (black) is plotted and guided by the two stable levels on each side of the melt zone. A soft dashed line connecting these levels has been suggested with error bars as the dark grey shaded area. The changes of the air content are caused by pressure changes due to changing surface elevation at the depositional sites and changes of air trapping processes in the firn assumed to be controlled by the changing summer insolation[28,32,49-51]. c) : When corrected for upstream flow (cyan) and summer insolation changes (green) the air content curve can be 'translated' to elevation changes (blue, dashed) with the shaded zone indicating the uncertainty range introduced by this translation.

Figure 1

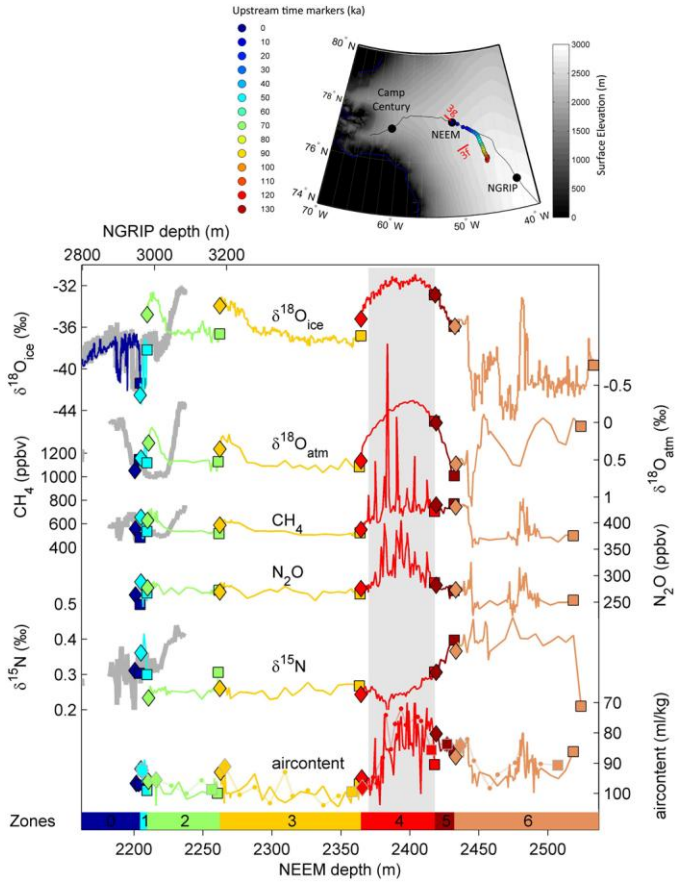
Upstream time markers (ka)
Camp Century
NEEM
NGRIP
Surface Elevation (m)
NGRIP depth (m)
NEEM depth (m)
δ18Oice
δ18Oatm
CH4
N2O
δ15N
aircontent
δ18Oice (‰)
CH4 (ppbv)
δ15N (‰)
δ18Oatm (‰)
N2O (ppbv)
aircontent (ml/kg)
Zones

Figure 2

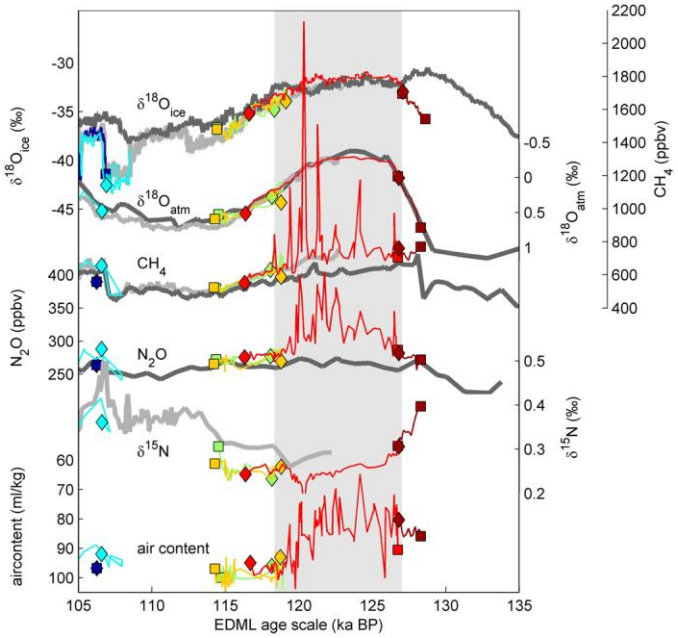
δ18Oice (‰)
δ18Oatm (‰)
CH4 (ppbv)
N2O (ppbv)
δ15N (‰)
aircontent (ml/kg)
δ18Oice
δ18Oatm
CH4
N2O
δ15N
air content
EDML age scale (ka BP)

Figure 3

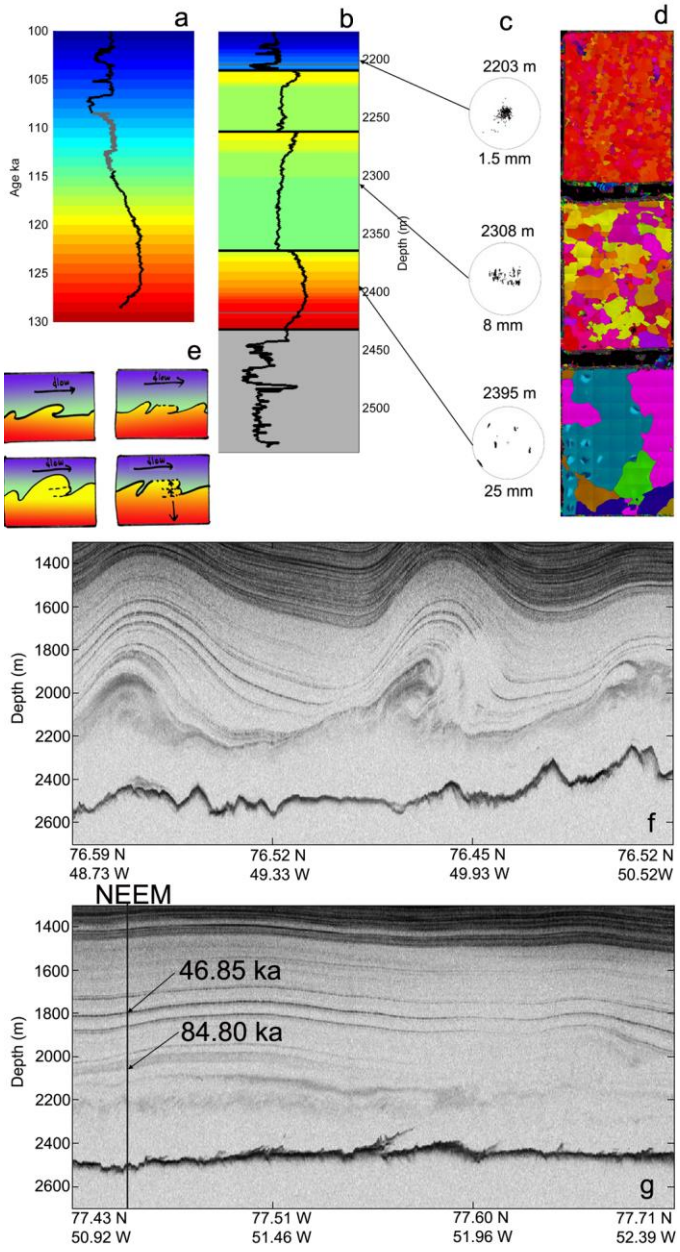
a
b
c
d
e
f
g
Age ka
Depth (m)
2203 m
1.5 mm
2308 m
8 mm
2395 m
25 mm
76.59 N
48.73 W
76.52 N
49.33 W
76.45 N
49.93 W
76.52 N
50.52W
NEEM
46.85 ka
84.80 ka
77.43 N
50.92 W
77.51 W
51.46 W
77.60 N
51.96 W
77.71 N
52.39 W

Figure 4

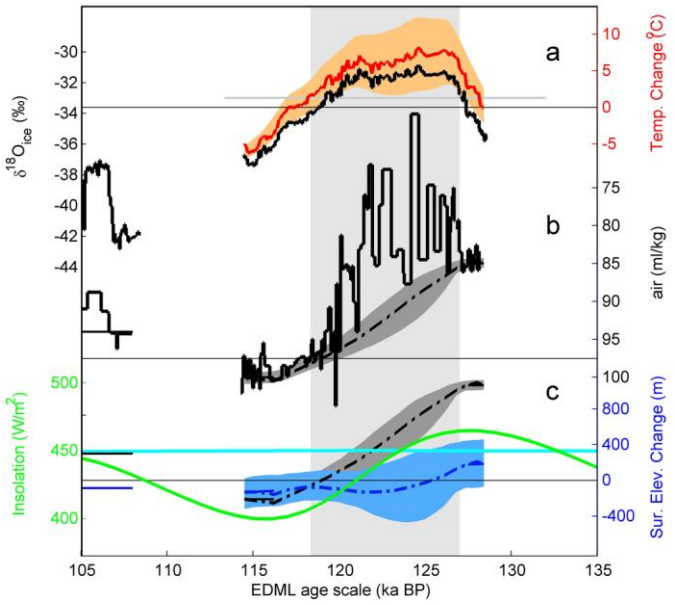
a
b
c
$\delta^{18}O_{ice}$ (‰)
Temp. Change (°C)
air (ml/kg)
Insolation (W/m²)
Sur. Elev. Change (m)
EDML age scale (ka BP)
-30
-32
-34
-36
-38
-40
-42
-44
10
5
0
-5
75
80
85
90
95
500
450
400
100
800
400
0
-400
105
110
115
120
125
130
135